Astron. Astrophys. 266, 202–214 (1992)

ASTRONOMY AND ASTROPHYSICS

Possible young stellar objects in the region of the Cygnus OB2 (VI Cygni) association from IRAS observations

M. Parthasarathy, S. K. Jain, and H. C. Bhatt

Indian Institute of Astrophysics, Bangalore 560034, India

Received July 17, 1990; accepted May 11, 1992

Abstract. From a study of the IRAS observations in the region of Cyg OB2 association 152 far infrared sources are detected. Of the 152 sources 97 have fluxes in two or more IRAS bands. Of these 97 sources 64 have positive spectral indices and steeply increasing flux towards longer wavelengths similar to that of young stellar objects (YSOs) embedded in thick dust shells. In addition there are 25 sources that have IRAS flux in one long wavelength band and low flux limit in a shorter wavelength band which yield a positive spectral index. Sources with positive spectral indices (YSOs) appear to have no optical counterparts. The dust temperatures and far infrared luminosities are derived for all the 97 sources. Most of the sources with positive spectral indices and flux distributions similar to YSOs have very cold (~ 40 K) dust shells. The far infrared luminosities range from a few 100 $L_\odot$ to a few times 10^3 or 10^4 $L_\odot$, which are expected luminosities of low mass ($\sim 1\ M_\odot$) and massive premain sequence stars respectively. Some of the very luminous ($\sim 10^4\ L_\odot$) sources have massive cold dust shells and are likely to be younger than ultra compact H II regions. The luminosity function for the IRAS sources in the Cyg OB2 suggests that most of the sources with positive spectral indices similar to YSOs are most likely members of the Cyg OB2 association. These results suggest that star formation is still taking place in Cyg OB2 association.

Key words: association – young stellar objects – premain sequence – dust – circumstellar matter – infrared radiation – early-type stars

1. Introduction

The Cygnus OB2 association (Cygnus II, VI Cygni) was found by Münch & Morgan (1953). OB associations in the region of Cygnus are listed by Humphreys (1978). The Cygnus OB2 association contains a group of very luminous and highly reddened ($A_v \sim 4$–10 mag) stars. It is very young, with members of spectral type as early as O3 (no. 7, Walborn 1973). The distance modulus of the association is between 10.9 and 11.6, probably 11.3 (Johnson & Morgan 1954, Reddish et al. 1967, Walborn 1973). Initially eleven OB stars were found by Münch & Morgan (1953). A further seven fainter OB stars were found by Morgan et al. (1954) using the technique of spectral classification by very low dispersion objective prism spectra. This technique was again applied to the region by Schulte (1956, 1958) who found ten more early type stars and a total of 88 suspected OB stars. Reddish et al. (1967) made *UBV* photographic photometry of about 1600 stars in the region of Cygnus OB2 association. They found more than 300 OB stars which are likely members of the association. Voelcker (1975) made *JHKL* photometric observations of about 103 stars. Some of the members of Cyg OB2 are particularly remarkable; for example, star no. 12 (Schulte 1958) (B5–8 Ia, $M_{\rm bol} = -10.9$) is one of the most luminous highly reddened ($A_v = 9.65$) stars (Rieke & Lebofsky 1985, Souza & Lutz 1980), star no. 9 is one of the most luminous O stars (O5 If, $M_{\rm bol} = -11.6$) and star no. 5 (V729 Cyg) is a contact binary with the primary O star ($M = 60\ M_\odot$) having one of the largest directly determined stellar masses known (Bohannan & Conti 1976, Leung & Schneider 1978).

Leitherer et al. (1982) found near infrared excesses in several of the Cyg OB2 stars. They atrribute this IR excess to free-free radiation of their expanding envelopes. Voelcker & Elsasser (1973, 1974), and Voelcker (1975) drew attention to the fact that the dust inside the Cyg OB2 association amounts to about 100 $M_\odot$ and its density is apparently higher at the center than at the outskirts. They estimated the amount of H II to be around $10^3\ M_\odot$ which is an order of magnitude less than expected from a normal gas to dust ratio of the interstellar medium if all hydrogen is ionized. Elsasser and Voelcker have concluded that all the observed interstellar extinctions of the stars can be explained by an interstellar dust cloud filling the volume of the association. It is then no longer possible to assume the existence of circumstellar dust shells around the OB stars in Cyg OB2 association. The Cyg OB2 association cannot be identified with a strong H II region which should surround an aggregation of many O-type stars. The O–B associations of age comparable to that of Cyg OB2 contain strong H II regions. The failure to detect any H II region associated with Cyg OB2 might be due to the lack of hydrogen. Huchtmeier and Wendker (1977) searched for radio continuum at 15 GHz from Cyg OB2. They found no compact H II region inside the Cyg OB2 association. They have argued that the lack of H II region in the Cyg OB2 association is due to the lack of neutral or molecular hydrogen inside the association.

YSOs have been detected in other associations with age comparable to that of Cyg OB2. Margulis et al. (1989) detected several young stellar objects in Monoceros OB1. Beichman et al. (1986) detected candidate solar-type protostars in nearby molecular cloud cores. Relatively massive YSOs have been detected by Persson & Campbell (1987) from IRAS data. The Cyg OB2 contains several massive very young O type stars and may contain

Send offprint requests to: M. Parthasarathy massive YSOs. In view of these interesting aspects of Cyg OB 2 we searched the IRAS point source catalogue to detect the far-infrared IRAS sources in the region of Cyg OB2 association. In this paper we report an analysis of the IRAS data for the sources in the direction of Cyg OB2 association.

2. IRAS observations

The Cyg OB2 association is centered around $\alpha = 20^h31^m.5$, $\delta = +41°16'$ (1950), $l = 80°.3$ and $b = +0°.8$, having an angular diameter of about 0°.8 corresponding to 30 pc in size at a distance of 2 kpc. We have searched the IRAS point source catalogue (Beichman et al. 1985) for far infrared sources within a circle of diameter 1° centered around the above mentioned central coordinates of Cyg OB2 association. The exact size of the association may be larger than 30 pc. Therefore, we have also searched the IRAS point source catalogue for far-infrared sources in a 2° diameter region of Cyg OB2 association. There is no overlap with any other associations within the 2° diameter region of Cyg OB2 association. The infrared sources detected within the 2° region centered around Cyg OB2 association are listed in Table 1. We have included all sources which were detected in any one or more wavelength bands. In all we found 152 sources. Of these 152 sources, 17 show fluxes at 12 μm, 25 μm, 60 μm and 100 μm. The uncertainties in the 12 μ, 25 μm, 60 μm and 100 μ fluxes of the sources are indicated in Table 1 by the side of the corresponding fluxes with the letters A, B, C, D, E, F corresponding to uncertainties of the order 4%, 8%, 12%, 16% and 20% respectively (Ref. IRAS point source catalogue and explanatory supplement).

3. Analysis

3.1. Far-IR sources

We have found 47 IRAS sources within a circle of diameter 1°. A preliminary discussion of these sources was reported earlier by Parthasarathy & Jain (1989). The IRAS data suggest the extent of the Cyg OB2 association to be larger than 1°. We have found 152 IRAS sources within an area with a diameter of 2° centered around Cyg OB2. Of the 152 sources 97 have fluxes in two or more IRAS bands. We have searched the IRAS low resolution spectra (LRS) catalogue (Olnon & Reimond 1986) and found LRS spectra for only 4 sources given in Table 1. The 12 μm to 100 μm flux distributions of several sources are shown in Fig. 1. The data shown in Fig. 1 suggests that many of the sources have steeply rising flux towards longer wavelengths which is one of the characteristic features of the YSOs.

Blaauw (1964) has shown that largest overall projected diameters of some of the associations are few hundred parsecs. To determine the size of the association photometric and astrometric data over a larger area is needed. Unlike star clusters an association gradually merges with the general field population. The concentration of several far infrared sources with steeply rising fluxes in the region of Cyg OB2 suggests that they are associated with the association. The locations of IRAS sources in the Cyg OB2 association are shown in Fig. 2. The numbers in Fig. 2 correspond to the numbers listed in Table 1.

The Cygnus OB2 association is a relatively crowded association. Reddish et al. (1967) found 400 stars brighter than $B = 16.5$ and their *UBV* photometry shows that at least 300 of them are OB stars. They also estimate that there are 900 stars brighter than $m_{pg} = 21$ and 3000 brighter than $m_r = 20$. No accurate RA and DEC coordinates are available even for some of the relatively bright stars in the Cyg OB2 association. Reddish et al. (1967) published x and y positions for about 1600 stars in the region of Cyg OB2 association. However, no accurate astrometric positions are available. Therefore, identifying the optical counterparts to IRAS sources is difficult. Many of the IRAS sources have no optical counterparts indicating that the optical counterparts are very faint or absent as a result of obscuration by the dust shells. Figure 2 should be used only to get an idea of the approximate locations of IRAS sources and their spatial distribution.

3.2. Spectral index (α_{IRAS})

The spectral indices of the IRAS sources given in Table 1 are computed from the equation (Margulis et al. 1989)

$$\alpha_{IRAS} = \frac{\log \lambda_1 F_{\lambda_1} - \log \lambda_2 F_{\lambda_2}}{\log \lambda_1 - \log \lambda_2}. \quad (1)$$

λ_1 is the short wavelength and λ_2 is the long wavelength at which IRAS flux has been detected. The spectral indices α_{IRAS} are listed in Table 1. If the flux is detected in all the four IRAS bands then $\lambda_1 = 12$ μm and $\lambda_2 = 100$ μm. If the flux quality or uncertainty in any of the IRAS bands is denoted by L (Table 1) (Ref. IRAS point source catalogue and explanatory supplement) then it is not used in calculating the spectral index (α_{IRAS}) and total far infrared flux. 28 sources of the total 152 have appreciable cirrus contribution (cirrus index > 5, Ref. IRAS point source catalogue and explanatory supplement) in the 100 μm band. We have not used the 100 μm fluxes of these 28 sources in computing the spectral index α_{IRAS}. The values of λ_1 and λ_2 used in computing α_{IRAS} are given in Table 1.

From an analysis of infrared flux distribution of sources in the star forming regions Lada & Wilking (1984) and Lada (1987) identified three distinct classes: Class I-sources with broader than blackbody energy distributions and rising flux longward of 2 μm. Class I sources are all invisible and deeply embedded in the dust cloud. The α index for class I sources is in the range of 0 to $+3$. Class II sources also have broader than blackbody energy distributions longward of 2 μm. Class II sources were classified as T Tauri stars. They have α index in the range 0 to -2. Most T Tauri stars (class II sources) have α index around $\alpha = -0.65$ to -1.0 (Rucinski 1985, Wilking et al. 1989). Class III sources have decreasing flux with increasing wavelength in the infrared. Their energy distributions could be modelled with reddened black bodies. The class III sources may have thin warm dust shells. Lada (1987) notes that class I objects are proto-stars. Recent models which predict the emergent energy distribution of low mass protostars clearly suggest that class I sources are indeed objects in the process of building up mass by the accretion of infalling circumstellar matter (Adams & Shu 1985). Class I sources have more circumstellar dust than class II sources and class I objects are at a much younger stage of development than class II sources.

3.2.1. Class I sources (possible YSOs)

The α_{IRAS} indices (Table 1) and flux distributions (Fig. 1) of many of the Cyg OB2 IRAS sources are in good agreement with the above descriptions of class I sources suggesting that a significant number of them are YSOs.

In the 47 sources within an area with a diameter of 1° there are 22 sources with positive spectral indices and 10 sources with negative spectral indices. The remaining 15 sources have flux in

Table 1. IRAS sources (in the region of Cyg OB2 association) and their dust temperatures and luminosities

S.	IRAS position	Flux density (Jy) 12 μm	25 μm	60 μm	100 μm	T_d (12/25 μm) (K)	T_d (25/60 μm) (K)	T_d (60/100 μm) (K)	α_{IRAS}	L_{IRAS} ($L_\odot$)		λ_1 (μm)	λ_2 (μm)
1	202732.9+403908	0.77 C	2.53 L	7.33 D	55.03 E(8)	–	–	27	+0.4	128		12	25
2	202733.9+402538	1.64 L	2.89 C	–	–	–	–	–	–	–		–	–
3	202735.2+400109	438.88 B	1111.92 B	5313.85 C	5689.43 D	203	81	66	+0.21	55621	RAFGL 2591	12	100
4	202735.3+413303	0.63 L	1.22 D	30.20 D	96.88 D(7)	–	58	35	+2.67	276		25	60
5	202739.9+412053	1.17 L	1.09 F	23.88 L	78.66 F(7)	–	–	–	–	–		–	–
6	202740.8+413040	29.45 B	11.04 B	–	–	770	–	–	−2.34	893	MWC 1021	12	25
7	202743.5+421047	0.63 C	0.85 D	7.25 C	47.34 D(8)	260	70	28	+0.51	125		12	60
8	202745.2+420059	0.67 C	0.63 F	7.96 F	–	310	65	–	+0.53	56		12	60
9	202746.5+411515	–	0.99 E	22.53 D	–	–	58	–	+2.57	101		25	60
10	202747.5+415419	0.91 L	0.80 L	11.38 D	–	–	–	–	–	–		–	–
11	202750.8+405542	2.05 B	1.51 C	–	–	370	–	–	−1.39	71	MRSL 079+113	12	25
12	202751.3+400805	1.58 C	2.47 D	–	–	243	–	–	−0.36	72		12	25
13	202806.8+403845	2.28 D	13.53 B	122.58 F	303.38 C(6)	157	70	40	+1.47	1164		12	60
14	202808.2+415720	–	1.02 F	17.95 F	–	–	60	–	+2.30	83		25	60
15	202810.6+410624	2.17 B	3.48 C	49.28 C	–	240	65	–	+0.96	291	MRSL 079+0113	12	60
16	202814.2+414705	1.74 L	2.02 L	15.84 D	–	–	–	–	–	–		–	–
17	202816.4+413734	1.75 L	2.59 L	6.88 D	–	–	–	–	–	–		–	–
18	202823.7+403102	0.70 D	–	–	–	–	–	–	–	–		–	–
19	202823.8+405723	1.77 L	1.25 F	16.39 C	–	–	65	–	+1.98	80		25	60
20	202832.1+421053	0.63 D	1.03 L	13.11 C	81.02 C(8)	–	–	30	+0.89	185		12	60
21	202833.0+404949	2.25 C	4.41 D	44.21 D	–	220	70	–	+0.85	289		12	60
22	202833.6+413348	2.79 B	1.68 C	–	–	440	–	–	−1.68	94		12	25
23	202834.5+403517	3.95 B	3.24 C	–	–	340	–	–	−1.27	143		12	25
24	202840.6+410539	12.91 D	91.90 B	789.89 D	1387.02 D	150	70	46	+1.21	6709	MRSL 079+0113	12	100
25	202843.6+415513	0.85 B	–	–	–	–	–	–	–	–		–	–
26	202844.6+402025	1.18 C	2.11 L	6.41 D	–	–	–	–	+0.04	55	DO 38486	12	60
27	202845.8+411352	1.01 L	2.55 L	14.54 L	52.59 C(8)	–	–	–	–	–		–	–
28	202854.7+411028	1.50 B	–	–	–	–	–	–	–	–		–	–
29	202859.7+412219	1.44 B	–	–	–	–	–	–	–	–		–	–
30	202901.1+403410	1.64 L	1.40 C	9.21 C	–	–	75	–	+1.15	55		25	60
31	202903.0+405215	0.58 F	5.62 C	65.67 E	136.29 D(7)	140	65	45	+1.94	547	MRSL 079+112	12	60
32	202903.5+403758	2.23 B	–	–	–	–	–	–	–	–		–	–
33	202906.4+420544	1.29 F	0.86 D	27.33 F	150.13 E(7)	395	55	30	+0.89	370		12	60
34	202909.4+413233	0.66 C	–	–	–	–	–	–	–	–		–	–

Table 1 (continued)

S.	IRAS position	Flux density (Jy) 12 µm	25 µm	60 µm	100 µm	T_d (12/25 µm) (K)	T_d (25/60 µm) (K)	T_d (60/100 µm) (K)	α_{IRAS}	L_{IRAS} ($L_\odot$)		λ_1 (µm)	λ_2 (µm)
35	202912.4 + 413501	5.60 E	3.46 E	–	–	420	–	–	−1.68	189		12	25
36	202913.4 + 410454	2.71 L	2.11 L	9.23 C	–	–	–	–	–	–		–	–
37	202915.6 + 404302	5.17 B	3.98 C	–	–	360	–	–	−1.33	189		12	25
38	202917.7 + 402056	0.98 C	–	–	–	–	–	–	–	–		–	–
39	202932.9 + 412630	0.46 D	2.08 L	7.42 C	–	–	–	–	+0.73	40		12	60
40	202942.0 + 405242	1.30 D	2.80 L	34.10 E	150.60 E (7)	–	–	32	+1.03	385	Cyg II-13	12	60
41	202946.0 + 405505	0.52 D	–	–	–	–	–	–	–	–		–	–
42	202957.2 + 421541	0.73 C	2.60 L	23.50 L	54.40 F (8)	–	–	–	–	–		–	–
43	203002.2 + 405847	2.01 L	6.08 C	47.59 F	159.09 F (7)	–	78	35	+1.35	504		25	60
44	203003.7 + 413915	11.80 B	8.87 B	–	–	360	–	–	−1.38	422		12	25
45	203010.7 + 401937	0.75 C	–	–	–	–	–	–	–	–		–	–
46	203018.8 + 414723	0.94 C	1.11 F	–	–	275	–	–	−0.79	39		12	25
47	203021.0 + 405544	3.23 C	3.71 C	–	–	280	–	–	−0.81	134		12	25
48	203022.6 + 403015	3.24 B	6.08 B	6.51 D	–	225	133	–	−0.56	192		12	60
49	203028.4 + 405900	4.21 B	10.29 B	179.80 C	800.20 E	205	57	33	+1.48	2119	ASS 21	12	100
50	203035.5 + 410808	1.74 B	1.10 C	–	–	410	–	–	−1.59	58	V 729 Cyg	12	25
51	203037.7 + 414607	1.01 D	1.44 D	36.02 L	119.29 C (7)	255	–	–	−0.54	220		12	25
52	203039.4 + 400550	71.79 L	547.77 C	7719.50 L	9979.30 C	–	65	56	+1.09	52181	RAFGL 2602	25	100
53	203044.6 + 401514	1.55 C	1.64 C	43.84 C	108.12 C (7)	295	57	40	+1.10	388		12	60
54	203046.5 + 420212	1.18 E	1.37 D	–	–	280	–	–	−0.79	50		12	25
55	203051.6 + 404957	0.62 D	–	–	–	–	–	–	–	–	DO 38536	–	–
56	203053.1 + 402315	–	–	9.20 E	–	–	–	–	–	–		–	–
57	203053.3 + 413422	1.63 C	3.22 C	–	–	225	–	–	−0.06	86		12	25
58	203053.4 + 410412	6.22 B	2.21 C	12.71 F	–	900	80	–	−0.55	236	Shulte 12 TMSS +40430 Cyg OB2 No. 12	12	60
59	203054.6 + 403153	1.72 L	8.69 B	–	–	–	–	–	–	–		–	–
60	203056.5 + 413800	0.89 D	2.43 E	–	–	198	–	–	+0.35	56		12	25
61	203101.5 + 402937	179.02 B	112.42 B	74.97 L	84.90 E (8)	420	–	–	−1.63	6206	MWC 349 RAFGL 2603	12	25
62	203103.0 + 414317	0.72 C	–	–	–	–	–	–	–	–	SAO 49769 G5	–	–
63	203104.6 + 415327	1.18 B	1.12 D	–	–	310	–	–	−1.12	46		12	25
64	203108.1 + 411051	0.83 D	1.03 L	11.03 F	–	–	–	–	+0.61	63	ASS 21	12	60

Table 1 (continued)

S.	IRAS position	Flux density (Jy) 12 µm	25 µm	60 µm	100 µm	T_d (12/25 µm) (K)	T_d (25/60 µm) (K)	T_d (60/100 µm) (K)	α_{IRAS}	L_{IRAS} ($L_\odot$)		λ_1 (µm)	λ_2 (µm)
65	203111.7+414707	–	–	10.54 E	–	–	–	–	–	–		–	–
66	203114.4+403535	183.94 C	131.09 B	70.52 L	–	380	–	–	−1.46	6470		12	25
67	203119.3+404041	1.29 L	1.82 D	9.73 C	–	–	80	–	+0.92	63		25	60
68	203122.3+414043	1.02 E	2.42 D	47.24 E	–	207	60	–	+1.39	241		12	60
69	203128.1+410651	1.78 C	4.08 L	61.26 D	–	–	–	–	+1.19	281	DO 19128	12	60
70	203130.3+404839	1.48 C	4.26 C	49.71 L	142.2 C(7)	195	–	–	+0.43	306	Near SAO 49784	12	25
71	203131.9+404635	1.19 L	3.01 E	–	–	–	–	–	–	–		–	–
72	203135.1+402625	2.09 B	–	–	–	–	–	–	–	–		–	–
73	203135.6+403708	0.63 C	7.06 B	70 L	96.16 F(7)	135	–	–	+2.30	258		12	25
74	203136.5+415519	1.16 D	1.74 D	24.38 L	151.42 F(7)	247	–	–	−0.53	276		12	25
75	203137.9+413922	0.65 D	2.14 C	–	–	185	–	–	+0.60	46		12	25
76	203139.8+403012	0.68 D	2.49 C	74.97 L	89.34 F(7)	180	–	–	+0.77	184		12	25
77	203142.5+415332	2.28 C	3.41 E	–	–	248	–	–	−0.47	106		12	25
78	203143.1+411506	1.05 F	2.02 L	26.05 E	–	–	–	–	+1.02	125		12	60
79	203145.3+410602	1.93 L	4.12 D	–	–	–	–	–	–		AS 427	–	–
80	203150.0+405946	1.50 C	–	–	–	–	–	–	–	–		–	–
81	203152.1+404213	1.64 L	2.36 L	19.47 F	–	–	–	–	–	–		–	–
82	203155.7+414527	1.11 L	2.50 F	–	–	–	–	–	–	–		–	–
83	203155.9+412029	0.57 C	–	–	–	–	–	–	–	–		–	–
84	203157.4+410357	2.98 C	2.55 C	–	–	–	–	–	−1.22	111		12	25
85	203200.1+420725	2.00 C	1.06 F	23.20 L	155.60 C(7)	480	–	–	−1.94	293		12	25
86	203200.7+413055	0.40 L	1.09 F	6.24 D	–	–	80	–	+0.98	40		25	60
87	203201.9+413607	0.83 B	–	–	–	–	–	–	–	–	SAO 49796	–	–
88	203202.7+420158	2.02 L	0.90 F	9.40 C	–	–	68	–	+1.68	49		25	60
89	203203.5+411509	–	2.47 E	–	–	–	–	–	–	–		–	–
90	203208.0+411222	5.20 B	28.30 B	427.90 D	920.61 C	160	65	41	+1.44	3533		12	100
91	203210.6+414610	1.58 L	2.52 E	–	88.72 D(7)	–	–	–	–	–		–	–
92	203215.2+421503	175.72 B	125.08 B	–	–	395	–	–	−1.46	6179	RAF 2609	12	25
93	203216.8+414252	0.48 C	–	–	–	–	–	–	–	–		–	–
94	203216.6+403101	0.92 C	6.35 C	23.96 F	–	151	87	–	+1.02	205		12	60
95	203226.3+405758	14.53 B	37.01 B	76.68 D	147.43 D(7)	200	100	45	+0.03	1400		12	60
96	203231.9+414115	0.36 C	3.56 F	23.12 E	–	138	75	–	+1.58	148	Cyg II-2	12	60
97	203233.7+421154	2.05 C	1.50 L	–	–	–	–	–	–	–		–	–
98	203234.7+413814	0.63 L	1.30 L	13.27 D	–	–	–	–	–	–		–	–
99	203243.5+412022	11.56 B	17.54 C	236.67 C	631.40 E	245	65	38	+0.89	2375		12	100
100	203246.0+414820	1.21 D	1.40 L	42.19 D	163.23 D(7)	–	–	34	+1.21	432		12	60

Table 1 (continued)

S.	IRAS position	Flux density (Jy) 12 µm	25 µm	60 µm	100 µm	T_d (12/25 µm) (K)	T_d (25/60 µm) (K)	T_d (60/100 µm) (K)	α_{IRAS}	L_{IRAS} ($L_\odot$)		λ_1 (µm)	λ_2 (µm)
101	203246.5+403703	1.54 L	4.61 L	37.42 E	–	–	–	–	–	–		–	–
102	203247.4+405527	2.28 B	4.12 L	20.41 D	–	–	–	–	+0.36	136	SAO 49823	12	60
103	203249.2+410621	1.05 D	4.44 E	–	–	173	–	–	+1.02	88		12	25
104	203252.8+404232	3.63 C	8.73 C	76.30 E	–	205	71	–	+0.90	508		12	60
105	203259.3+410425	0.73 B	3.93 F	–	–	160	–	–	+1.34	73		12	25
106	203300.6+410957	0.64 D	6.40 C	77.90 L	131.60 E(7)	138	–	–	+2.14	300		12	25
107	203305.3+402758	2.11 B	14.73 B	–	–	150	–	–	+1.65	261		12	25
108	203306.6+402442	7.38 A	35.70 C	127.12 D	–	167	35	–	+0.77	1182		12	60
109	203309.1+405322	0.57 E	–	–	–	–	–	–	–	–		–	–
110	203312.3+403439	1.20 L	2.50 L	45.60 L	125.72 D(7)	–	–	–	–	–		–	–
111	203312.8+402144	0.85 F	–	–	–	–	–	–	–	–		–	–
112	203312.9+412424	11.44 B	77.46 C	909.21 D	1376.07 F	151	68	51	+1.26	6909		12	100
113	203320.0+420004	1.11 L	1.43 L	23.63 E	–	–	–	–	–	–		–	–
114	203321.3+410253	22.85 D	74.88 B	1246.12 E	2471.62 C	185	61	44	+1.21	10066		12	100
115	203322.5+412758	3.22 B	–	–	–	–	–	–	–	–		–	–
116	203323.2+403133	0.46 L	4.29 E	–	–	–	–	–	–	–		–	–
117	203323.6+415315	0.57 L	0.56 L	9.38 C	–	–	–	–	–	–	SAO 49835	–	–
118	203331.4+414301	0.83 B	–	–	–	–	–	–	–	–		–	–
119	203331.5+405915	0.35 L	5.51 F	–	–	–	–	–	–	–		–	–
120	203331.9+402636	0.66 C	5.92 D	–	–	143	–	–	+1.98	100		12	25
121	203335.9+404730	1.29 B	–	–	–	–	–	–	–	–		–	–
122	203343.8+403608	1.91 B	6.38 C	41.64 C	–	185	76	–	+0.92	299		12	60
123	203346.5+410456	4.42 B	7.80 D	192.37 F	542.43 D	232	58	38	+1.27	1758		12	100
124	203347.8+405201	0.44 L	3.56 C	31.29 E	–	–	70	–	+1.50	170		25	60
125	203350.4+404834	0.40 L	2.50 E	–	–	–	–	–	–	–		–	–
126	203351.0+405557	3.59 C	9.61 B	57.09 D	–	200	76	–	+0.72	447		12	60
127	203351.3+410248	1.99 F	–	–	–	–	–	–	–	–		–	–
128	203351.3+403025	0.39 L	2.14 D	–	–	–	–	–	–	–		–	–
129	203357.5+414724	0.58 L	1.06 L	10.40 F	–	–	–	–	–	–		–	–
130	203359.6+411220	0.99 B	–	–	–	–	–	–	–	–	BD +40° 4243	–	–
131	203401.2+402203	0.38 L	2.55 E	–	–	–	–	–	–	–		–	–
132	203401.5+401753	0.76 B	–	–	–	–	–	–	–	–		–	–
133	203406.8+404721	7.52 B	4.49 E	–	–	440	–	–	−1.70	252		12	25
134	203407.6+410327	2.21 F	6.13 L	59.74 F	149.06 F(7)	–	–	39	+1.05	504		12	60
135	203412.7+413916	0.69 F	1.01 E	–	–	250	–	–	−0.49	31		12	25
136	203419.5+412933	22.12 B	151.76 B	690.20 E	1035.34 E	151	82	50	+0.81	6889		12	100
137	203420.0+401923	3.94 B	–	–	–	–	–	–	–	–		–	–

Table 1 (continued)

S.	IRAS position	Flux density (Jy) 12 µm	25 µm	60 µm	100 µm	T_d (12/25 µm) (K)	T_d (25/60 µm) (K)	T_d (60/100 µm) (K)	α_{IRAS}	L_{IRAS} ($L_\odot$)	λ_1 (µm)	λ_2 (µm)
138	203423.4+412341	1.68 D	1.63 C	27.32 D	–	310	61	–	+0.72	170	12	60
139	203430.6+404818	3.10 B	4.31 D	–	–	255	–	–	−0.55	139	12	25
140	203434.7+402419	0.31 L	2.66 D	13.47 E	–	–	80	–	+0.88	89	25	60
141	203446.9+404042	0.88 B	3.23 L	53.24 L	80.40 C(7)	–	–	–	–	–	–	–
142	203451.3+412719	3.01 F	–	–	–	–	–	–	–	–	–	–
143	203502.8+405544	0.59 C	8.04 D	51.45 D	98.60 F(7)	130	76	45	+1.77	471	12	60
144	203504.8+412602	14.53 E	171.10 B	1280.66 E	3241.54 D	135	74	39	+1.55	12488	12	100
145	203504.9+403027	1.46 B	2.86 D	47.46 D	–	220	62	–	+1.19	258	12	60
146	203505.4+410438	1.23 C	2.08 C	15.68 E	–	235	75	–	+0.60	120	12	60
147	203510.4+412146	3.31 B	–	–	–	–	–	–	–	–	–	–
148	203512.9+412424	6.13 B	32.94 C	–	–	160	–	–	+1.30	620	12	25
149	203513.5+411432	0.45 L	2.09 L	18.38 E	–	–	–	–	–	–	–	–
150	203516.8+413041	4.09 D	2.90 F	–	–	377	–	–	−1.47	144	12	25
151	203534.9+401959	0.63 E	–	–	–	–	–	–	–	–	–	–
152	203535.5+412454	1.50 C	2.40 D	–	–	240	–	–	−0.36	72	12	25

The numbers in the parenthesis in the 100µm flux column are cirrus flags (Ref. IRAS explanatory supplement)

only one band, and therefore no spectral index could be computed. We have mentioned earlier that the exact size of the association is uncertain. However, IRAS data suggest that the diameter of the association is of the order of 2°. We have found 152 IRAS sources within an area with a diameter of 2° centered around Cyg OB 2. Of the 152 sources 97 have fluxes in two or more IRAS bands. Of these 97 sources 64 have positive spectral indices and 29 have negative spectral indices. Sources with positive indices are most likely YSOs. All the sources with positive spectral indices have steeply rising fluxes towards longer wavelenghts. Most of the class I sources (positive spectral indices) could not be identified with definite optical counterparts. The optical counterparts may be very faint or could be obscured by dust envelopes.

We have searched the IRAS point source catalogue in an adjacent region to Cyg OB 2 in a square of area 1 square degree centered at $\alpha = 20^h40^m\!.8$, $\delta = +41°$ and found 8 IRAS sources, most of which have low fluxes. Only 3 of these 8 have flux distributions characteristic of class I sources. Compared to the surface density of class I sources in this region (3 sources per square degree), the Cyg OB 2 region has a source density 23 per square degree of class I objects. This suggests that an overwhelming majority of class I sources found in the Cyg OB 2 region are YSOs and are members of the association.

The α index of Lada & Wilking (1984) and Lada (1987) and Lada's classes I, II and III are based on infrared flux distribution in the wavelength region typically 2 µm to 10 µm. Our α_{IRAS} index is based on IRAS data. For the IRAS sources in the Cyg OB 2 region we do not have near IR (2 µm to 10 µm) fluxes to compute α_{Lada}. However, IRAS sources classified as class I, and class II based on the IRAS data (α_{IRAS}) were also found to belong to the same class when classified using the near IR (2 µm to 10 µm) data (α_{Lada}) (Kenyon et al. 1990, Wilking et al. 1989).

We have found 64 sources which have positive spectral indices and steeply increasing flux towards longer wavelengths (class I) similar to that of young stellar objects. Most of the evolved giants and carbon stars show far infrared flux decreasing from 12 µm to 100 µm. The number density of evolved giants and carbon stars is too low to account for the 64 class I sources within 2° field of Cyg OB 2. Wendker et al. (1991) made a detailed investigation of radio continuum structure on large and small scales in the Cygnus X region. They conclude that the association is young and that no supernova has occurred within it. They also conclude that there are no individual H II regions in Cyg OB 2 association. The presence of several possible young stellar objects suggests that they are members of Cyg OB 2 and the association is relatively young with an age of less than 10^6 years.

3.2.2. Class II sources (embedded T Tauri stars)

From a study of IRAS data of known T Tauri stars Rucinski (1985) found that the IRAS spectral indices (α_{IRAS}) of these stars are around -0.55 and only very rarely greater than zero. Margulis et al. (1989) found several IRAS sources with negative spectral indices (α_{IRAS}) in Monoceros OB 1 which they attribute to T Tau stars. Wilking & Lada (1983), Lada (1987), Wilking et al. (1989) suggest that infrared sources with α index in the range 0 to -2 are likely to be T Tauri stars. Margulis et al. (1989) suggest that the dividing line between class III and II is about spectral index (α_{IRAS}) of -2.5, and the dividing line between classes II and I is about spectral index (α_{IRAS}) of zero. In the Cyg OB 2 region we find 29 sources with negative spectral indices (Table 1). Of these 29 sources 21 have α_{IRAS} indices in the range 0 to -1.5 which can be classified as class II sources. Most of these class II sources could

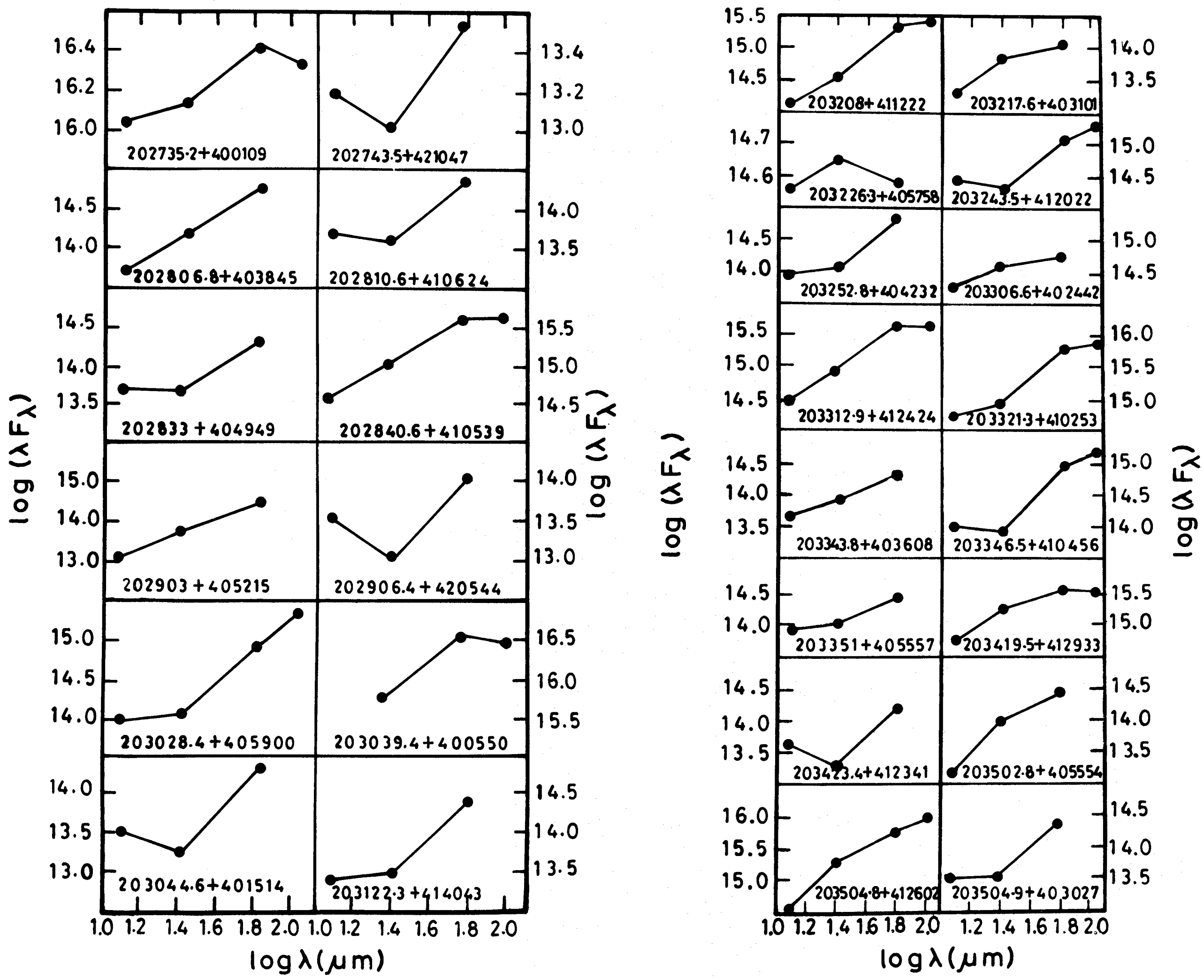

Fig. 1. The far infrared (12μm to 100μm) flux distributions of class I (positive spectral index) sources in the region of Cyg OB2 association

not be identified with definite optical counterparts. The optical counterparts may be very faint or could be obscured by dust envelopes. Of the 21 class II sources in Cyg OB2 region a significant fraction may be considered as embedded T Tauri stars. The number of class I sources in the Cyg OB2 region is much higher than the number of class II sources.

4. Dust around a few O–B stars

The Cyg OB2 association contains a large number of relatively bright OB stars. The majority of these stars are still on the main sequence (Massey & Thompson 1991). Majority of the O–B stars do not show infrared (IRAS) excesses indicating absence of cold shells around them. However V729 Cygni, Cyg OB2 number 12 and MWC 349 were found to be IRAS sources.

4.1. *V729 Cygni*

The IRAS source no. 50 (Table 1) is found to be associated with the O-type massive close binary V729 Cygni (Bohannan & Conti 1976), which shows flux densities 1.74 Jy and 1.1 Jy at 12 μm and 25 μm respectively. The IRAS observations of V729 Cygni suggest the presence of dust around the system. The temperature and far-infrared luminosity of the dust are estimated to be 410 K and 58 $L_{\odot}$, respectively. The dust around V729 Cyg (Cyg OB2 no. 5 = BD+40°4220) is likely to be a remnant of the matter from which V729 Cyg was formed. However V729 Cyg shows stellar wind and mass loss (Hutchings 1981; Vreux 1985) and the secondary component may be an evolved star which has experienced mass loss (Bohannan & Conti 1976), and the presence of warm dust can also be attributed to the mass loss from the system.

4.2. *Cyg OB2 number 12*

Another optical candidate which is identified with an IRAS source is Cyg OB2 no. 12. Star no. 12 stands out from the rest of the association in several ways. As pointed out by Bohannan (1975), it is the only late B star known in the association, which is dominated by O-type stars. It has by far the largest reddening, with $B-V$ colour excess of $3^{m}.25$ (Johnson 1968) compared with a mean of $\sim 1^{m}.8$ (Schulte 1958) for the association. Its absolute magnitude M_V is between −9.3 and −10.0, making it one of the brightest known stars in the Galaxy (Sharpless 1957; Souza & Lutz 1980). Souza & Lutz (1980) confirm the spectral type and luminosity class of Cyg OB2 no. 12 to be B8 Ia. They also confirm the

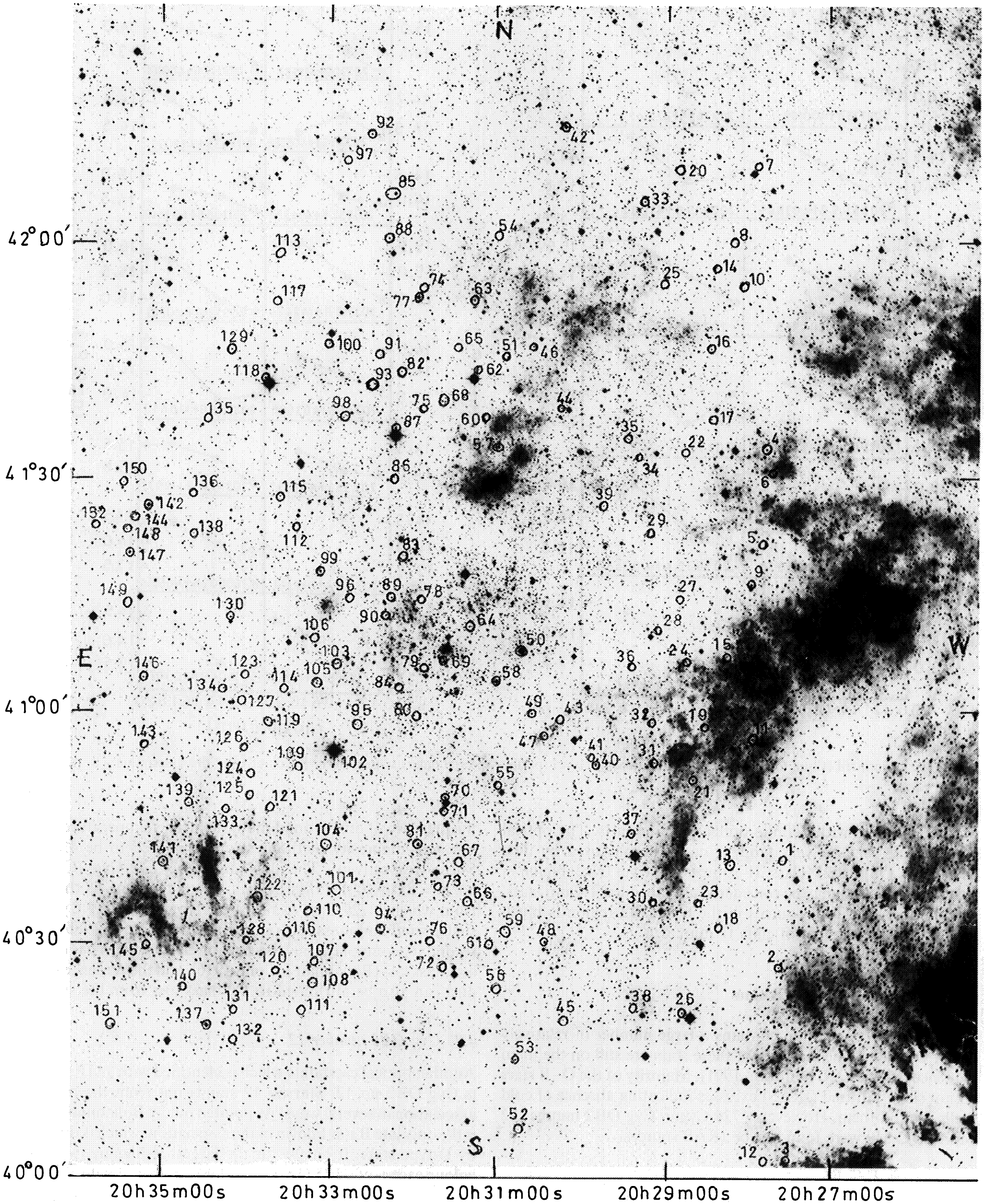

Fig. 2. The location of IRAS sources in the region of Cyg OB2 association

membership of this star and suggest that it may be a binary. This star shows stellar wind mass loss (Hutchings 1981; Souza & Lutz 1980). The IRAS fluxes at 12 μm, 25 μm, and 60 μm of Cyg OB2 no. 12 are 6.22 Jy, 2.21 Jy and 12.71 Jy, respectively. The IRAS fluxes suggest the presence of warm dust (~ 900 K) and cold dust (80 K) around this star, and the far infrared luminosity is $236\,L_\odot$.

4.3. *MWC 349*

The IRAS source 203101.5+402937 is identified with the peculiar Be star MWC 349. The low resolution spectrum (LRS) is featureless. The nature and evolutionary status of MWC 349 is not clear, it may be a young or an evolved object. Recent observations suggest that MWC 349 is a bipolar nebula with a hot object at the center; the central hot object appears to be a binary (White & Becker 1985; Cohen et al. 1985). The IRAS flux distribution of MWC 349 is different from that of young stellar objects; it shows flux maximum around 12 μm. The dust temperature T_d is of the order of 400 K and the far infrared luminosity $L_\mathrm{IRAS} = 0.62\ 10^4\,L_\odot$, assuming a distance of 2 kpc. The IRAS source 202740.8+413040 is identified with MWC 1021. It has a dust temperature of 770 K and far infrared luminosity $L_\mathrm{IRAS} = 8.9\ 10^2\,L_\odot$. The IRAS sources 203114.4+403535 and IRAS 203215.2+421503 show large flux in the 12 μm and 25 μm bands; they may be emission line objects similar to MWC 349 and MWC 1021. These sources have negative spectral indices and are likely to be associated with emission line stars.

5. Completeness of the survey

Since we have used only the IRAS point source catalogue the completeness of the list in Table 1 may be questionable. The list of infrared sources given in Table 1 is by no means complete. We may have missed some of the extended sources and also some of the bright sources in the point source catalogue may be really extended and/or multiple. Because of relatively large size of IRAS beams the resolution is low and several of the bright sources may be unresolved double or multiple sources. Very bright sources may be missed because of a large lobe, and also hide nearby weaker sources. In particular, faint sources situated very near bright, discrete sources may have been missed due to confusion. For example, in IRAS maps of ϱ Ophiuchi and Mon OB1 region Wilking et al. 1989, Margulis et al. 1989, found beams as large as several arcmin in the cross-scan direction. They also found evidence for the presence of large structures (Wilking et al. 1989). Margulis et al. (1989) in their study of Mon OB1 demonstrated that the use of IRAS maps and filtering (see Figs. 1 and 2 of Margulis et al. 1989) can resolve this problem and detect more sources compared to the use of IRAS point source catalogue. Therefore our list of infrared sources (Table 1) is a lower limit to the total number of infrared sources in the region of Cygnus OB2. Unfortunately we do not have IRAS maps and near and mid-IR array camera observations of Cyg OB2 region to resolve and detect more sources.

6. Colour–colour diagram

The far infrared colour-colour diagram is shown in Fig. 3. In the log (S_{25} μm/S_{60} μm) vs. log (S_{12} μm/S_{25} μm) plot there are very few sources in the region of T Tau stars. The distribution of sources in the colour-colour diagram is similar to that found by Beichman et al. (1986), Clemens & Barvainis (1988), Berrilli et al. (1989) and Braz & Epchtein (1987) for YSOs.

The YSOs identified by Persson & Campbell (1987) and Beichman et al. (1986) are also shown in Fig. 3. The Cyg OB2 sources occupy the region defined by the YSOs in the far infrared colour-colour diagram. There are a few sources (Fig. 3) with log (S_{12} μm/S_{25} μm) colour greater than -0.2 which may not be YSOs. The colour-colour diagram suggests that most of the class I sources in the region of Cyg OB2 (Table 1) are most likely YSOs.

7. Luminosities (L_IRAS) and temperatures (T_d) of the dust shells

The far infrared (in the IRAS bands) luminosities of these sources are computed using the following equation (Margulis et al. 1989):

$$\frac{L_\mathrm{IRAS}}{L_\odot} = 3.76\ 10^2 \left[\frac{F_{12\,\mu\mathrm{m}}}{(12\,\mu\mathrm{m})^2} (18.5\,\mu\mathrm{m} - 8.75\,\mu\mathrm{m}) + \frac{F_{25\,\mu\mathrm{m}}}{(25\,\mu\mathrm{m})^2} (52.5\,\mu\mathrm{m} - 18.5\,\mu\mathrm{m}) + \frac{F_{60\,\mu\mathrm{m}}}{(60\,\mu\mathrm{m})^2} (80\,\mu\mathrm{m} - 42.5\,\mu\mathrm{m}) + \frac{F_{100\,\mu\mathrm{m}}}{(100\,\mu\mathrm{m})^2} (119.67\,\mu\mathrm{m} - 80\,\mu\mathrm{m}) \right]. \tag{2}$$

The factor 60.1 in the Margulis et al's (1989) equation for Monoceros OB1 and the factor $3.76\ 10^2$ in the above equation for Cyg OB2 are constants proportional to the square of distance to the associations (800 pc for the Mon OB1 and 2 kpc for the Cyg OB2 association). The IRAS luminosities L_IRAS are listed in Table 1. Most of the sources have steeply increasing fluxes towards longer wavelengths. A single temperature cannot represent the flux distribution which is a common characteristic of dust embedded sources. Therefore, colour temperatures based on 12 μm–25 μm, 25 μm–60 μm and 60 μm–100 μm colours are computed and are given in Table 1. The 12 μm–25 μm colours yield the dust temperature of the order of few 100 K and the 60 μm–100 μm colours yield dust temperatures of the order of 30 to 40 K. For the 28 sources with appreciable cirrus contribution (cirrus flag > 5) in the 100 μm band (Table 1) the dust temperature from the 60 μm to 100 μm flux ratio will be a lower limit. The cirrus also affects the evaluation of the infrared luminosities of these 28 sources. For these the 100 μm band flux listed in Table 1 is an upper limit. Therefore, the IRAS luminosities of these 28 sources could be lower by a factor of 1.5 to 2 than those listed in Table 1. However, the general conclusions drawn in the present analysis are not affected by these corrections to a few sources.

The far infrared luminosities in the IRAS bands L_IRAS of the class I and class II sources (Table 1) considered here are found to range from $\sim 40\,L_\odot$ to $\sim 10^4\,L_\odot$. McCutcheon et al. (1991) from an analysis of 7 μm to 6 cm fluxes of a few massive protostellar candidates find that the far infrared IRAS luminosities of protostellar candidates can be $\sim 42\%$ lower if only 12 μm to 100 μm fluxes are considered. They have shown that this underestimate of luminosity is however balanced by an overestimate of luminosity because the duplicity or multiplicity of the IRAS protostellar candidates is not known and it has not been taken into account in estimating far IR luminosities as the IRAS fluxes have been attributed to a single source. A similar argument applies to the IRAS luminosities of the sources considered here. Therefore

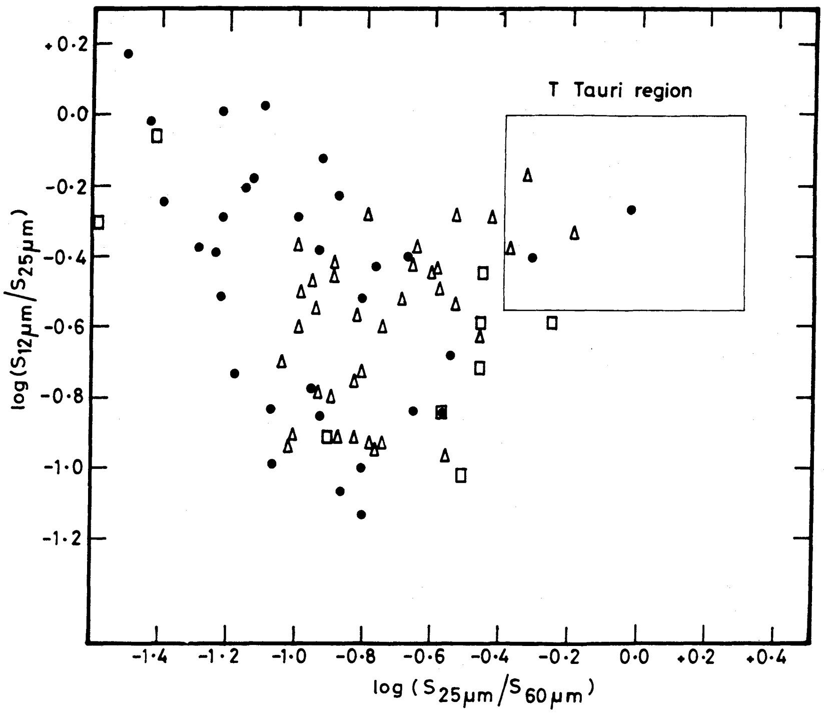

Fig. 3. The colour-colour (12 µm/25 µm and 25 µm/60 µm) diagram of infrared sources in the region of Cyg OB2 association. The symbol △ represents the YSOs detected by Persson and Campbell (1987) and the symbol □ represents the YSOs detected by Beichman et al. (1986)

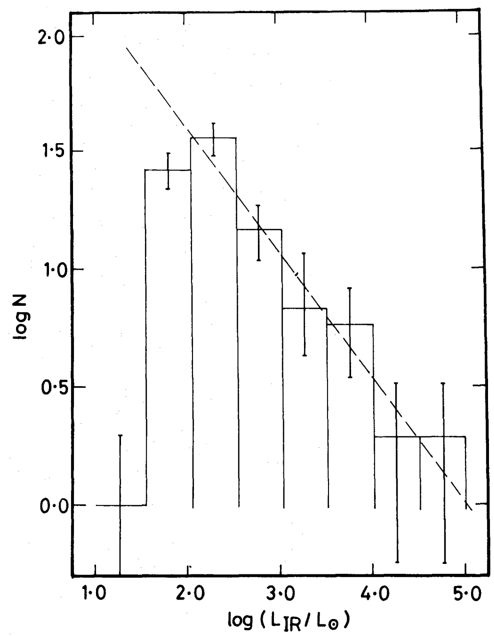

Fig. 4. The luminosity function for the IRAS sources in the Cyg OB2 association. N is the number of sources in a given luminosity bin. The error bars represent the statistical fluctuation $\sqrt{N}$ in N

the IRAS luminosities of the class I sources listed in Table 1 are nearly equal to their bolometric luminosities.

7.1. Luminous IRAS sources

Sources nos. 49, 90, 95, 99, 112, 114 (Table 1) have high luminosities and are most likely massive YSOs. The solar mass protostars are expected to have luminosities upto the order of 60 $L_\odot$ (Stahler et al. 1980; Adams et al. 1987). Some of the sources with far-infrared luminosities less than 60 $L_\odot$ may be low mass embedded T Tau stars. Optical identification, spectroscopy and near infrared photometry of these sources (Table 1) may enable us to understand their nature.

The five sources (Table 1) IRAS 20324+4057, 20327+4120, 20332+4124, 20333+4102, and 20343+4129 are within 16′ of one another, and are close to the center of the Cyg OB2 association. According to the CO survey by Cong (1980), the CO cloud identified as "source 47" is adjacent to IRAS 20327+4120 and has a distance of 2 kpc and a total mass of 2 10^4 $M_\odot$. This CO cloud is within Cyg OB2 association. The IRAS source in this group which appears to be relatively more massive than the above mentioned sources is IRAS 20333+4102. The far-infrared flux distributions of this source and other sources mentioned above are shown in Fig. 1. This source has an IRAS luminosity $L_{IRAS} \simeq 10^4 L_\odot$. The flux distribution is matched with that of massive YSOs. Another luminous source in this region is IRAS 20343+4129. The far IR luminosity is 6.9 10^3 $L_\odot$. These five sources lie within the region of CO cloud of Cyg OB2 association and are most likely massive YSOs. CO $j=1\rightarrow0$ and $2\rightarrow1$ millimeter wave observations of these sources may enable us to detect the molecular outflows and possible bipolar nature of these objects. The far infrared luminosities of these sources are close to their bolometric luminosities and correspond to the luminosities of early type stars. The IRAS sources 203202+405847, 203028+405900, 203130+404839 and 203208+411222 have far infrared energy distributions similar to that of massive YSOs. The far IR luminosities of these four sources are 5 10^2 $L_\odot$, 2.1 10^3 $L_\odot$, 3.1 10^2 $L_\odot$ and 3.5 10^3 $L_\odot$ respectively.

The LRS spectrum of IRAS source 202735.1+400109 shows silicate absorption features at 10 µm and 18 µm. The LRS spectrum, the 12 µm, 25 µm, 60 µm and 100 µm flux distribution (Table 1, Fig. 1) and the far IR luminosity of 5.6 10^4 $L_\odot$ suggest that it is a deeply embedded YSO. It is not in the list of ultra compact H II regions. It may be younger than an ultra compact H II region. The low resolution 8 µm–22 µm spectrum of IRAS 202802.8+403845 is rather flat and noisy between 8 µm to 22 µm. The IRAS source 202840.6+410539 also shows 10 µm silicate absorption feature. The far infrared flux distribution and luminosity ($L_{IRAS} = 0.67$ 10^4 $L_\odot$) (Fig. 1, Table 1) suggest that it is a YSO.

7.2. *Low luminosity sources*

Since the Cyg OB2 association is at a distance of 2 kpc, the far IR fluxes from low luminosity and low mass YSOs cannot be detected. The IRAS observations of Cyg OB2 revealed mostly the YSOs of high and intermediate mass range. There could be several solar mass protostars in the Cyg OB2 region similar to that detected by Margulis et al. (1989) in Monoceros OB1 molecular cloud.

The Monoceros OB1 is relatively near (800 pc) compared to Cyg OB2 (2 kpc). To detect the low mass protostars in Cyg OB2 region one requires a much more sensitive survey.

8. Luminosity function

In Fig. 4, we show the luminosity function for the IRAS sources in the Cyg OB 2 association. The least square fit to the histogram excluding the two lowest luminosity bins is $\log N = m \log L + b$ with $m = -0.52 \pm 0.01$ and $b = 2.63 \pm 0.03$. The slope of -0.52 is almost equal to that found by Berilli et al. (1989) for IRAS sources exciting molecular outflows. It is to be noted that the sources in Berilli et al. do not belong to a single cluster or association and have different and uncertain distances. Figure 4 thus indicates that the luminosity function of the YSOs within this single OB association (at 2 kpc) is the same as that of YSOs in the solar neighbourhood. Because of the large distance to Cyg OB 2 association IRAS detection of low luminosity sources ($L_{\rm IRAS} < 10^2 L_\odot$) would be incomplete. For this reason we have excluded the low luminosity bins. Extrapolating the luminosity function to lower luminosities it is found that the total number of YSOs with $L_{\rm IRAS} > L_\odot$ in the Cyg OB 2 association is ~ 450.

The value -0.52 for the slope of the luminosity function found here supports strongly the assumption that the IRAS sources are indeed association members, all at the same distance. If the IRAS sources were simply field objects at varying distances in this direction, the expected slope for a flux limited sample would be -1.5.

To convert the luminosity function into mass function for stars we require a knowledge of the mass luminosity relation. If the Cyg OB 2 IRAS sources follow the same mass luminosity relation as that adopted by Berilli et al (1989) for outflow driving YSOs in the solar neighbourhood then the mass function for the YSOs in Cyg OB 2 association should be similar to that of the outflow driving YSOs in the solar neighbourhood because their luminosity functions are similar. Berilli et al. (1989) found the cumulative mass function for the outflow driving YSOs, which gives the number of sources with mass greater than M to be a power law with a power index $\Gamma = -1.8 \pm 0.2$. This is not significantly different from the initial mass function for the stars in the solar neighbourhood.

The mass function for the IRAS sources in the Cyg OB 2 association as indicated by their luminosity function cannot, however, be taken as the mass function for the entire association. This is because only a small fraction of the association members are IRAS sources. There is a large number of massive OB-type stars in the Cyg OB 2 association that are not IRAS sources. The IRAS sources found in this study are YSOs with masses in the range $\sim 1 M_\odot$ to $\sim 10 M_\odot$ as derived from the mass-luminosity relation given in Berilli et al. (1989). Recently the population of massive stars in the Cyg OB 2 association was studied by Massey & Thompson (1991) using CCD *UBV* photometry and spectroscopy. For stars in the mass range $\sim 10 M_\odot$ to $\sim 85 M_\odot$ they found a mass function considerably flatter ($\Gamma = -1.0 \pm 0.1$). For masses $\leqq 15 M_\odot$ the sample is affected by incompleteness.

Massey & Thompson (1991) found the initial mass function (IMF) of Cyg OB 2 to be considerably flatter than that previously found for massive stars in the Galaxy and for most regions studied in the LMC. However,our analysis of IRAS data suggests a steeper slope. Garmany et al. (1982) found evidence of a gradient in the slope of the IMF with galactocentric distance for massive stars within the Milky way. With a galactic longitude of 80°, Cyg OB 2 has a galactocentric distance nearly equal to that of the Sun. If Garmany et al. (1982) "gradient" in IMF is correct then we expect a steeper slope of IMF which is in agreement with our result, but not in agreement with the flatter slope derived by Massey & Thompson (1991). However, Garmany et al's (1982) result of gradient in the slope of the IMF is controversial (see Massey 1985, Scalo 1986). Massey & Thompson (1991) note that the IMF of Cyg OB 2 is similar to the flatter IMF found for LH 10 in the LMC. However, two studies of IMFs in LMC clusters have appeared recently in the literature: Mateo (1988), and Elson et al. (1989). Mateo find steeper IMFs (steeper than that of solar neighbourhood clusters) for six LMC clusters, while Elson et al. report exceptionally flat IMFs for a different sample of six clusters, drawn from roughly the same population. Possible sources of discrepancy are incompleteness of data, inclusion of evolved stars and undetected close binary stars. The flat IMF for Cyg OB 2 derived by Massey & Thompson and steeper IMF suggested from our analysis of YSO, both these studies suffer from incompleteness of data. Massey & Thompson study is based upon smaller area of the Cyg OB 2 association. The discrepancy may be due to differences in the range of masses of the stars involved. Massey & Thompson derived the IMF of Cyg OB 2 based on stars in the mass range $10 M_\odot$ to $85 M_\odot$ while most of our YSOs may be in the mass range $10 M_\odot$ to $1 M_\odot$. Some of the YSOs in our sample may be double or multiple which we have considered as single sources. Also non-coeval star formation may be one of the reasons for the difference in IMFs.

It is possible that the mass function of Cyg OB 2 cannot be represented by a single power law and that stars with masses in different mass ranges were formed at different times. Indeed there is evidence for non-coeval star formation in Cyg OB 2. Massey & Thompson (1991) found that a few slightly evolved supergiants of lower mass are present in Cyg OB 2 suggesting that star formation in the association was not strictly coeval. The IRAS detections of YSOs discussed here clearly shows that the star formation process in Cyg OB 2 is still continuing. A study of the entire association along the lines of Massey & Thompson (1991) and near and mid IR study of infrared sources (Table 1) is needed for a better understanding of this association.

9. Conclusions

From an analysis of the 12 μm to 100 μm flux data of IRAS sources in the region of Cyg OB 2 association we find several massive young stellar objects. We find 64 sources with positive spectral indices and steeply increasing far infrared flux distribution similar to that found in known young stellar objects. Some of these sources have massive cold dust shells with far infrared luminosities of the order of $10^3 L_\odot$ to $10^4 L_\odot$ and are most likely massive young stellar objects which may show bipolar structure and molecular outflows. The luminosity function for the IRAS sources in the Cyg OB 2 suggests that most of the sources with positive spectral indices are most likely members of the Cyg OB 2 association. The extent of the Cyg OB 2 association is of the order of 2° in diameter. The absence of compact and ultracompact H II regions in the Cyg OB 2 suggests that the IRAS sources with far infrared luminosities of the order of $10^4 L_\odot$ are younger than ultra compact H II regions. Since the distance of Cyg OB 2 is 2 kpc the IRAS survey has sampled mostly luminous or relatively massive young stellar objects in this region. The observed luminosity distribution (Fig. 3) suggests that there may be a few hundred low mass (of the order of solar mass) young stellar objects in the Cyg OB 2 association.

In order to know the exact size (angular diameter) of Cyg OB 2 assocation we need to extend the survey of IRAS sources to include a larger area around Cyg OB 2, say a diameter of 4°. However, the problem one encounters be extending to 4° diameter is possible inclusion of outer regions of nearby associations like Cyg OB8 and Cyg OB9 etc. Study of IRAS maps and CO isophotes [along the lines of Wilking & Lada (1983) in their study of ϱ Oph cloud] of this region may help to determine the size of this association. Also, with CCD *UBV* photometry of the field with a 4° diameter centered around Cyg OB2 it is possible to detect many new OB stars and their colour magnitude diagrams and radial velocity observations may enable us to derive the exact extent of this association.

The star formation mechanisms in OB associations are not yet clearly understood. Blaauw's (1964) study indicates that about 30% of the OB associations have recognizable sub-groups of different ages. Recent studies of star forming regions suggest that stimulation could still be important for the formation of very massive stars. The work of Klein et al. (1980) and Sugitani et al. (1989) suggest that shocks from ionization fronts stimulate star formation. The distribution of IRAS sources in the Cyg OB2 region suggests that there are regions of relatively dense gas and dust and massive stars are still forming. In these regions there may be low mass young stellar objects which are not yet detected. The analysis of the sources considered here applies in each case to a single stellar object. The dust and gas clouds surrounding some of the bright sources may well enclose a group or cluster of protostars. The duplicity or multiplicity of the sources and the exact number of YSO in the Cyg OB2 region will be known from high resolution IR imaging, CO observations, etc.

Acknowledgements. We are thankful to the referee for his critical comments which helped to improve the presentation of the paper.

References

Adams F.C., Shu F.H., 1985, ApJ 296, 655
Adams F.C., Lada C.J., Shu F.H., 1987, ApJ 312, 788
Beichman C.A., Neugebauer G., Habing H.J., Clegg P.E., Chester T.J., 1985, IRAS Point source Catalogue, JPL
Beichman C.A., Myers P.C., Emerson J.P., Harris S., Mathieu R., Benson P.J., Jennings R.E., 1986, ApJ 307, 337
Berrilli F., Ceccarelli C., Liseau R., Lorenzetti D., Saraceno P., Spinoglio L., 1989, MNRAS 237, 1
Blaauw A., 1964, Ann. Rev. Astr. Ap. 2, 213
Bohannan B., 1975, AJ 80, 625
Bohannan B., Conti P.S., 1976, ApJ 204, 797
Braz M.A., Epchtein N., 1987, A & A 176, 245
Clemens D.P., Barvainis R., 1988, ApJS 68, 257
Cohen M., Bieging J.H., Dreher J.W., Welch W.J., 1985, ApJ 292, 249
Cong H., 1980, Ph. D. Thesis, Columbia University
Elson R.A.W., Fall S.M., Freeman K.C., 1989, ApJ 336, 734
Garmany C.D., Conti P.S., Chiosi C., 1982, ApJ 263, 777
Huchtmeier W.K., Wendker H.J., 1977, A & A 58, 197
Humphreys R.M., 1978, ApJS 38, 309
Hutchings J.B., 1981, PASP 93, 50
Johnson H.L., 1968, in: Nebulae and Interstellar Matter, eds. B. M. Middlehurst & L. H. Aller, University of Chicago Press, Chicago, p. 191
Johnson H.L., Morgan W.W., 1954, ApJ 119, 344
Kenyon S.J., Hartmann L.W., Strom K.M., Strom S.E., 1990, AJ 99, 869
Klein R.I., Sandford M.T., Whitaker R.W., 1980, Space Sci Rev. 27, 275
Lada C.J., 1987, in: Star forming regions, IAU Symp. No. 115, eds., M. Peimbert, J. Jagaku, Dordrecht, Reidel, p. 1
Lada C.J., Wilking B.A., 1984, ApJ 287, 610
Leitherer C., Hefele H., Stahl O., Wolf B., 1982, A & A 108, 102
Leung K.C., Schneider D.P., 1978, ApJ 224, 565
Margulis M., Lada C.J., Young E.T., 1989, ApJ 345, 906
Massey P., 1985, PASP 97, 5
Massey P., Thompson A.B., 1991, AJ 101, 1408
Mateo M., 1988, ApJ 331, 261
McCutcheon W.H., Dewdney P.E., Purton C.R., Sato T., 1991, AJ 101, 1435
Morgan W.W., Meinel A.B., Johnson H.M., 1954, ApJ 120, 506
Münch L., Morgan W.W., 1953, ApJ 118, 161
Olnon F.M., Raimond E., 1986, A & A 65, 607
Parthasarathy M., Jain S.K., 1989, Interstellar dust, IAU Symp. No. 135, contributed papers, NASA Conference publication 3036, p. 211
Persson S.E., Campbell B., 1987, AJ 94, 416
Reddish V.C., Lawrence L.C., Pratt N.M., 1967, Publ. Roy. Obs. Edinburgh 5, 111
Rieke G.H., Lebofsky M.J., 1985, ApJ 288, 618
Rucinski S.M., 1985, AJ 90, 2321
Scalo J.M., 1986, Fundam. Cosmic Phys. 11, 1
Schulte D.H., 1956, ApJ 124, 530
Sharpless S., 1957, PASP 69, 239
Souza Sp.P., Lutz B.L., 1980, ApJ 235, L87
Stahler S.W., Shu F.H., Taam R.E., 1980, ApJ 241, 637
Sugitani K., Fukui Y., Mizuno A., Ohashi N., 1989, ApJ 342, L87
Voelcker K., 1975, A&A 22, 1
Voelcker K., Elsasser H., 1973, in: Interstellar dust and related topics, IAU Symp. No. 52, Dordrecht, Reidel, p. 529
Voelcker K., Elsasser H., 1974, Mem. Soc. Astron. Ital. 45, 295
Vreux J.M., 1985, A & A 143, 209
Walborn N.R., 1973, ApJ 180, L35
Wendker H.J., Higgs L.A., Landecker T.L., 1991, A & A 241, 551
White R.L., Becker R.H., 1985, ApJ 297, 677
Wilking B.A., Lada C.J., 1983, ApJ 274, 698
Wilking B.A., Lada C.J., Young E.T., 1989, ApJ 340, 823